Desalination and Water Treatment
www.deswater.com
50 (2012) 411–422
December

doi: 10.1080/19443994.2012.744718
Taylor & Francis
Taylor & Francis Group

Effects of concentration polarization, temperature and pressure on ultrasound detection of inorganic fouling and cleaning in a spiral-wound membrane module

G.Y. Chai[a], Bing Cao[a], G.Y. Zhao[a], Alan R. Greenberg[b,*], W.B. Krantz[c]

[a]*College of Materials Science and Engineering, Beijing University of Chemical Technology, Beijing 100029, China*
[b]*Department of Mechanical Engineering, NSF Center for Membrane Science, Engineering and Technology, University of Colorado, Boulder, CO 80309-0427, USA*
Tel. +1 303 492 6613; Fax: +1 303 492 4637; email: alan.greenberg@colorado.edu
[c]*Singapore Membrane Technology Center, Nanyang Technological University, Singapore 639798, Singapore*

Received 2 August 2012; Accepted 25 October 2012

ABSTRACT

Ultrasonic time-domain reflectometry (UTDR) involves passing an acoustic wave through a medium and analyzing the reflected waveform. In this study, UTDR is used to track the waveform peaks reflected from the outer and inner membranes in the outermost feed channel in a Koch 2521 spiral-wound module. The UTDR amplitude is shown to be more sensitive to fouling than the transit (arrival) time. The local (point) measurement provided by UTDR is shown to be advantageous since its location can be optimized for early fouling detection. Concentration polarization is shown not to compromise UTDR. This is an advantage relative to flux decline that responds to both fouling and concentration polarization. The UTDR amplitude is found to increase with increasing temperature and decreasing pressure. This is explained by the effect these parameters have on the crystallization rate that changes the fouling layer morphology and thereby the reflected UTDR waveform. This study underscores the importance of establishing a UTDR reference surface suitable for unambiguous detection of fouling. It also emphasizes the necessity for good temperature and pressure control during UTDR measurements as well as a more comprehensive understanding of the effects of operating condition changes on the ultrasound waveforms.

Keywords: Ultrasonic time-domain reflectometry; Fouling; Spiral-wound module; Calcium sulfate; Reverse osmosis

1. Introduction

Fouling is a major problem in membrane processes that significantly increases the cost or limits the use of membranes for water treatment and other liquid separation processes. Scaling is a form of fouling that involves precipitation of sparingly soluble inorganics. It is a major problem in applying membrane technology for high-pressure membrane processes such as the use of reverse osmosis (RO) and nanofiltration (NF) for desalination. A comprehensive review of scale formation in high-pressure membrane water treatment systems has recently been published by Antony et al. [1]. There is a need for methods both for monitoring membrane fouling and cleaning for large-scale water-treatment processes and to provide fundamental information on the fouling process via laboratory-scale studies. This paper focuses on the use

*Corresponding author.

of ultrasonic time-domain reflectometry (UTDR) as a technique for monitoring fouling, in particular scaling, noninvasively in real time. The principles of UTDR will first be reviewed after which a brief summary is given of prior studies that have applied UTDR to study membrane fouling.

The principles and theory underlying the use of ultrasound are discussed in detail in standard references such as Krautkramer and Krautkramer [2]. Reviews of the use of ultrasound for characterizing membranes and membrane processes have been given by Greenberg and Krantz [3] and Krantz and Greenberg [4]. UTDR is based on the principle that an acoustic wave is affected by the media through which it travels. In the pulse-echo mode, a sound wave is transmitted and reflected from the various interfaces in the medium of interest (e.g. a membrane module). The instantaneous amplitude of the reflected waveform is measured as a function of time. The resulting waveform is a spectrum of peaks corresponding to primary and multiple reflections from the interfaces encountered by the sound wave. Changes in the amplitude and transit (arrival) time of the various peaks in the waveform can provide information on events occurring within the medium such as membrane fouling. UTDR involves analyzing the reflected waveform in the time domain, whereas ultrasonic frequency-domain reflectometry analyzes the reflected waveform in the frequency domain.

An ultrasound wave is created by electrically exciting a piezoelectric device rigidly attached externally to the object being studied (e.g. membrane module), which in the pulse-echo mode acts as both the wave transmitter and reflected waveform receiver. An ultrasound wave propagates via compression and rarefaction of the material through which it travels; hence, its velocity c is a property of this material and is generally proportional to the density. For the media encountered in a spiral-wound module, $c \cong$ 1,500 m/s for water, 2,000 m/s for a polymer, and 2,600 m/s for an epoxy resin. When an ultrasound wave encounters an interface between two media, reflection, transmission, and mode-conversion (i.e. phase angle change between incident and reflected waves) can occur. The magnitude of the reflected and transmitted waves is determined by the acoustic impedance difference between the media on either side of an interface $Z_2 - Z_1$, where $Z_i \equiv \rho_i c_i$ in which the subscripts 1 and 2 denote the media from which and into which, respectively, the wave is propagating. For an incident wave perpendicular to an interface, the amplitude A of the reflected relative to the incident wave is given by

$$A = \frac{Z_2 - Z_1}{Z_2 + Z_1} \tag{1}$$

If $Z_2 > Z_1$, the reflected and incident waves will be in phase, whereas if $Z_2 < Z_1$, they will be 180° out-of-phase. Higher frequency ultrasound waves are more responsive to changes in the media, but are more strongly attenuated, which makes resolving their reflections more difficult. Hence, the choice of the ultrasound transducer frequency is a compromise between sensitivity and attenuation. Current ultrasound technology for membrane applications uses transducers in the 1–25 MHz frequency range that permits noninvasive, real-time characterization with micron-scale resolution.

UTDR was first applied to membrane processes by Bond et al. [5] who used it to measure membrane compaction under high pressure. Subsequent applications of UTDR to study membrane compaction were done by Peterson et al. [6], Reinsch et al. [7], Aerts et al. [8], and Kelley et al. [9]. UTDR has also been used to study membrane formation noninvasively in real time by Kools et al. [10]. The first use of UTDR to study membrane fouling was that of Mairal et al. [11,12] who studied calcium sulfate dihydrate scaling on a flat-sheet RO membrane in the cross-flow mode. Mairal's results were confirmed by Sanderson et al. [13]. Li et al. [14] used UTDR to study calcium sulfate fouling on flat-sheet RO membranes in both the cross-flow and dead-end modes. Silica fouling on flat sheet RO membranes was studied using UTDR by Chong et al. [15]. Zhang et al. [16] and Chai et al. [17] were the first investigators to apply UTDR to monitor calcium sulfate scaling in a commercial 2¼-inch (5.6 cm) spiral-wound RO module. Recent applications of UTDR to monitoring calcium sulfate scaling in a commercial 4-inch (10.2 cm) spiral-wound module have been done by An et al. [18,19]. Calcium sulfate scaling has been studied using UTDR for flat sheet NF membranes by Zhang et al. [20] and Cobry et al. [21], and calcium carbonate scaling by Li et al. [22]. Calcium sulfate and microbial synergistic fouling on flat sheet NF membranes has been studied by Hou et al. [23]. Li et al. applied UTDR to study bovine serum albumin fouling on flat sheet UF membranes [24] and on tubular UF membranes [25]. Li et al. [26] and Li and Sanderson [27] applied UTDR to study kaolin particle fouling on flat sheet microfiltration (MF) membranes and Xu et al. [28] used UTDR to study kaolin particle fouling on tubular MF membranes. Sanderson et al. [29] applied UTDR to monitor fouling on a flat sheet MF membrane used to treat a paper mill effluent. Sikder et al. [30] used UTDR to monitor the fouling

caused by natural brown water from a municipal reservoir. Silalahi et al. [31] applied UTDR to monitor fouling associated with the use of a flat-sheet MF membrane to separate oil-in-water emulsions. Recently, Sim et al. [32] have used UTDR to monitor fouling by colloidal silica on flat-sheet MF membranes.

Particularly noteworthy among the aforementioned studies is the development of three complementary ways to analyze the UTDR data. Chai et al. [17] were able to measure the instantaneous local thickness of the scaling deposits by tracking the specific peaks associated with the UTDR reflections from the outermost layers in a spiral-wound module. Zhang et al. [16] developed the concept of the "acoustic signature" characterized by comparing either the arrival time or amplitude of the peaks for the fouled spiral-wound module to those of the same module prior to fouling. Sanderson et al. [29] developed a "Fourier wavelet" approach whereby the waveform in the time domain is transformed into the frequency domain in order to compare the fouled and unfouled ultrasound response for the same membrane. The acoustic signature and Fourier wavelet approaches are advantageous for using UTDR in a control scheme strategy whereby a quantifiable metric is required to determine when some appropriate action should be taken. For example, Lu et al. [33] and Mizrahi et al. [34] recently employed changes in acoustic signature to control flow reversal to mitigate scaling in RO desalination. Analyzing specific peaks may be more useful for fundamental studies of membrane fouling where one seeks to determine the nature of fouling at specific locations and times in the membrane module.

All the aforementioned studies involved using acoustic transducers fixed rigidly to the membrane module at one or more fixed locations. An alternative approach involves using scanning acoustic microscopy (SAM) whereby the acoustic transducer is scanned over the surface of the object. Kujundzic et al. [35] used SAM to study fouling during MF of an industrial fermentation broth. Since SAM permits using higher frequency transducers that provide better resolution, it can be used to study biofouling for which the acoustic impedance difference between the biofouling layer and the membrane is quite small. However, SAM requires immersing the membrane in a suitable coupling agent such as water. As such, it cannot be applied for noninvasive real-time detection of fouling in commercial membrane modules.

This paper builds on prior studies by employing the analysis of specific peaks associated with the UTDR waveform to study calcium sulfate dihydrate scaling in a spiral-wound RO membrane module. UTDR is used to follow a complete cycle of fouling and cleaning. Apparent disparities between flux decline and recovery and the UTDR response are explained. The ability of UTDR to distinguish between flux decline owing to scaling and that due to concentration polarization is also demonstrated by employing sparingly soluble calcium sulfate dihydrate to cause fouling and soluble sodium chloride to cause concentration polarization in the absence of any fouling. Limited exploratory studies of the effects of temperature and pressure on UTDR detection of the scaling process are also presented.

2. Materials and methods

The commercial spiral-wound RO modules (Koch 2521) that were used in these membrane fouling and cleaning studies have a length and diameter of 47.7 and 5.6 cm, respectively. The modules have 12 concentric envelope layers, each feed channel of which contains two membranes. Fig. 1 shows a schematic of a cross-section of a 2521 spiral-wound membrane module.

The fouling agent was calcium sulfate dihydrate (Aldrich 98%). Feed solutions with concentrations up to 1.6 g/L were prepared using deionized distilled water. The flow system had a circulating volume of 12 L and consisted of the spiral-wound RO membrane module, a feed tank with temperature control, standard devices for the control and measurement of pressure, feed concentration, flow rate, and temperature. A low-pressure pump was used to transport the feed through a 2 m prefilter and then to a high-pressure booster pump. The retentate and permeate from the module were recycled to the feed tank to ensure stable operation. A new module was preconditioned by flowing pure water for 20 h to remove the protective

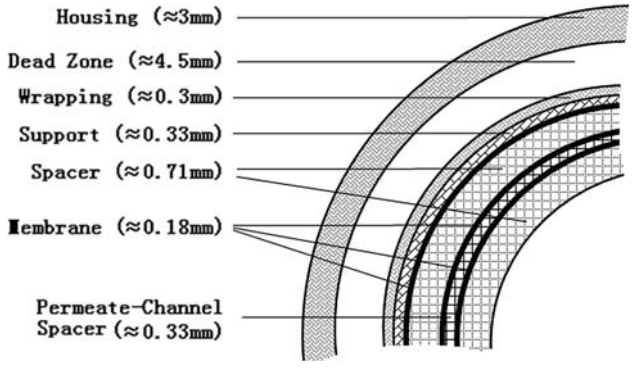

Fig. 1. Schematic of a cross-section of a 2521 spiral-wound membrane module.

coating from the membranes. The standard operating procedure was to run at the maximum test pressure for at least one hour prior to an experiment in order to minimize subsequent membrane compaction effects.

The UTDR hardware included a custom-made 3.5 MHz focused transducer, a pulser-receiver (Panametrics 5052PRX) and a digital storage oscilloscope (Nicolet Pro 50). The UTDR technique involves placing one or more transducers on the outside of the module housing and using the pulse-echo mode of operation. One of the UTDR transducers was located 14 cm from the retentate–effluent end of the module where the concentration polarization would be more significant. The UTDR response signal was continuously sampled and stored on a personal computer. The sampling rates permitted storing 1,000 data points to represent the reflected UTDR waveform.

The experimental protocol for the fouling and cleaning cycle experiments involved first having a deionized distilled water-feed during which both the permeate flux and UTDR response were measured. The feed then was abruptly changed to an aqueous solution of calcium sulfate that caused fouling, flux decline, and a UTDR response. The feed then was abruptly changed back to deionized distilled water, which gradually began to dissolve the calcium sulfate deposits during which the permeate flux and UTDR response were continuously measured. A moderate transmembrane pressure of 0.68 MPa was used so that the permeation flux would not be too large. This in turn ensured a relatively slow fouling rate and provided a more sensitive test of the UTDR methodology.

The procedure for demonstrating that UTDR measurements are not compromised by concentration polarization effects involved starting with a deionized distilled water-feed during which both the permeate flux and UTDR response were measured. The feed then was abruptly switched to an aqueous solution of sodium chloride, which caused concentration polarization but did not foul the membrane. The feed then was abruptly switched back to deionized distilled water, which quickly swept out the salt solution that was causing the concentration polarization.

The effect of temperature and pressure on the UTDR response to membrane fouling was studied by systematically increasing the temperature of the feed while holding the transmembrane pressure constant and by increasing the transmembrane pressure while holding the temperature constant.

3. Results and discussion

Fig. 2 shows a representative UTDR waveform. Three peaks denoted by A, B, and C were selected from this waveform and were tracked during the fouling and cleaning processes. Peak A is the ultrasonic echo signal from the outer wrapping of the membrane module; this peak was selected to determine whether the membrane element was stable or responding in

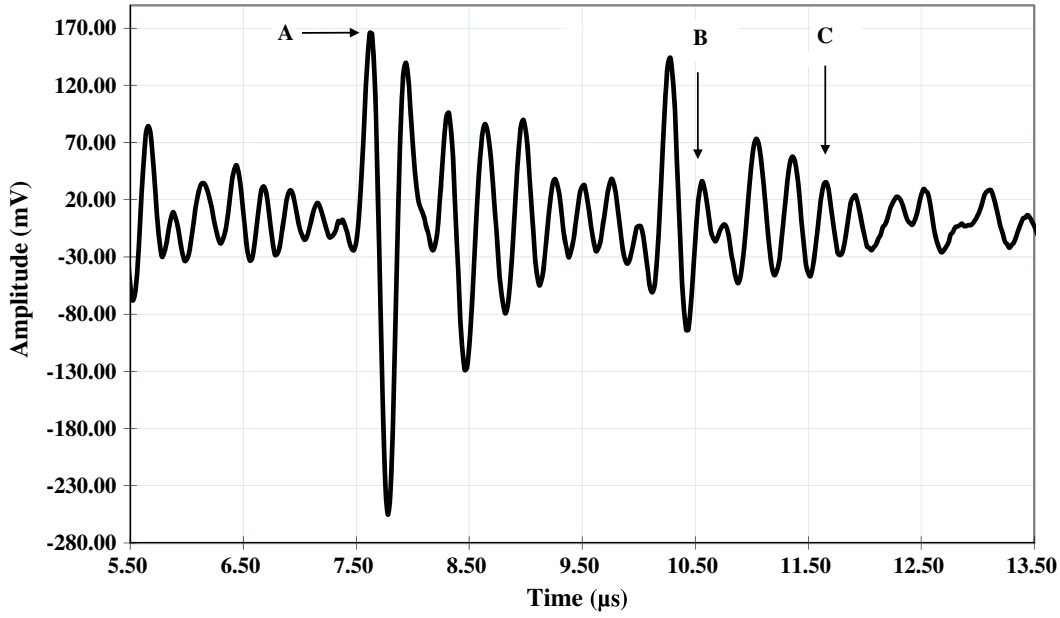

Fig. 2. Representative UTDR waveform: peak A from outer wrapping material, peaks B and C emanate from the outer and inner membranes in the outermost feed channel of the 2521 spiral-wound module.

some way to module expansion since it is unaffected by the fouling process. Peaks B and C emanate from the outer and inner membranes in the outermost feed channel in the 2521 spiral-wound module. These peaks were identified from the waveform response by determining the interfaces from which they were reflected using the appropriate acoustic velocities [17].

3.1. Complete fouling and cleaning cycle

Table 1 summarizes the results from a complete fouling and cleaning cycle at a pressure of 0.68 MPa and a temperature of 20˚C that include the operating time, permeation flux normalized with respect to the initial deionized distilled water value, calcium sulfate concentration in the feed, rejection, UTDR amplitude normalized with respect to the deionized distilled water value for peaks A, B, and C, and the UTDR arrival time for peaks A, B, and C. Fig. 3 shows a plot of the normalized flux on the left ordinate axis and the normalized amplitudes of peaks B and C on the right ordinate axis as a function of time (note the different ordinate scales). After the module was preconditioned for 1 h at the operating pressure of 0.68 MPa, a deionized distilled water feed was introduced during which time the permeation flux and amplitudes of peaks B and C maintained constant values as can be seen from the data in Table 1 and Fig. 3. At 27.5 h (shown by the vertical dotted line on the left in Fig. 3), the feed was abruptly changed to a 1.6 g/L solution of calcium sulfate after which membrane fouling began. This fouling caused a decline in the permeation flux, a decrease in the amplitude of peak B and an increase in the amplitude of peak C. This contrasting amplitude behavior arises because the ultrasound wave passes through the membrane into the fouling layer for peak B, but through the feed solution into the fouling layer for peak C for the feed channel configuration in a spiral-wound module; that is, the interface that causes the primary reflection of the ultrasound waveform is dramatically different for peaks B and C. At 76 h (shown by the vertical dotted line on the right in Fig. 3), the feed was abruptly switched back to deionized distilled water, which caused the calcium sulfate fouling layer to gradually dissolve. This dissolution is manifested by an increase in the permeation flux, an increase in the amplitude of peak B, and a decrease in the amplitude of peak C. Note that the permeation flux returns to nearly its initial value prior to introducing the calcium sulfate solution, whereas the amplitudes of peaks B and C do not return to their initial values. This seemingly inconsistent behavior arises because the permeation flux is an integral measure of the fouling throughout the

Table 1
Performance data for a complete cycle of fouling and cleaning for calcium sulfate fouling of a 2521 spiral-wound RO module at a pressure of 0.68 MPa and temperature of 20˚C

Phase	Time (h)	Normalized flux (%)	$CaSO_4$ in feed (g/L)	Salt rejection (%)	Normalized UTDR amplitude (%)			UTDR arrival time (μs)		
					Peak A	Peak B	Peak C	Peak A	Peak B	Peak C
H_2O	12.0	100.0	0.01	97.4	100.0	100.0	100.0	7.62	10.56	11.66
	22.5	98.9	0.01	97.9	98.9	100.0	100.0	7.62	10.56	11.66
	27.5	100.0	0.01	98.3	100.1	98.5	109.5	7.62	10.56	11.66
Fouling	28.5	98.2	0.73	99.7	99.6	95.5	114.3	7.62	10.56	11.66
	38.5	74.2	1.52	99.6	102.0	91.3	127.9	7.60	10.52	11.62
	57.0	71.5	1.53	99.6	102.1	87.7	128.8	7.60	10.52	11.62
	64.5	71.3	1.36	99.2	101.1	78.0	129.5	7.58	10.52	11.62
	70.0	73.2	1.35	99.0	97.3	76.3	130.2	7.58	10.50	11.60
	72.0	73.8	1.38	99.14	95.5	65.1	138.0	7.38	10.30	11.40
	76.0	73.6	1.33	99.2	96.1	65.6	133.8	7.40	10.30	11.40
Cleaning	81.5	84.1	0.71	98.7	103.9	72.7	127.6	7.38	10.30	11.40
	82.5	88.2	0.67	98.9	103.0	71.2	126.2	7.38	10.30	11.40
	86.5	89.2	0.85	98.6	86.1	72.7	121.4	7.40	10.34	11.44
	90.0	93.5	0.29	98.8	89.0	73.9	123.8	7.40	10.32	11.44
	94.0	96.1	0.15	98.8	100.1	90.1	115.2	7.40	10.34	11.42
	96.0	97.6	0.05	98.7	98.9	90.1	114.3	7.40	10.32	11.42
	100.5	98.9	0.03	97.8	99.0	90.1	111.9	7.40	10.34	11.44
	103.0	98.5	0.03	98.9	99.3	92.4	109.5	7.40	10.34	11.42

entire membrane module, whereas UTDR provides a local value. The ultrasonic transducer was purposely located at a point where fouling would be maximized, namely at the downstream end of the module. Fig. 3 clearly indicates that at this downstream point, the calcium sulfate fouling layer was still not totally dissolved. Hence, since UTDR responds to local conditions in the membrane module via an effective

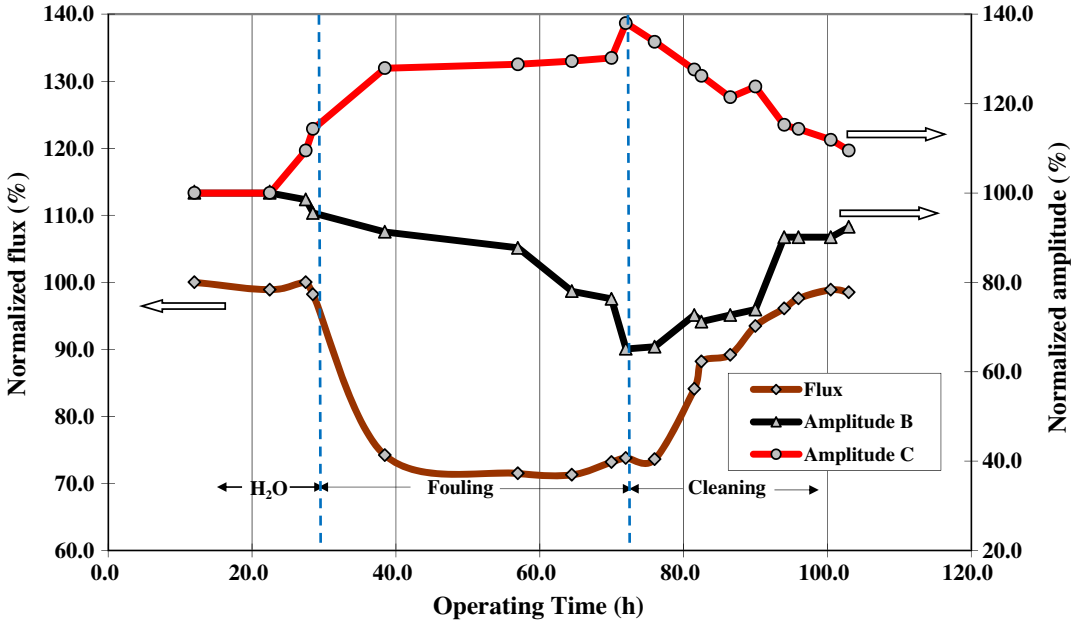

Fig. 3. Normalized permeation flux (left ordinate) and normalized UTDR waveform amplitude for peaks B and C (right ordinate) as a function of time for a complete cycle of calcium sulfate fouling and cleaning at a pressure of 0.68 MPa and temperature of 20°C; the feed was deionized distilled water until 27.5 h (vertical dotted line on left), at which time it was switched to a solution of 1.6 g/L of calcium sulfate that caused membrane fouling; at 76 h, the feed was switched back to deionized distilled water (vertical dotted line on right) that progressively dissolved the fouling layer.

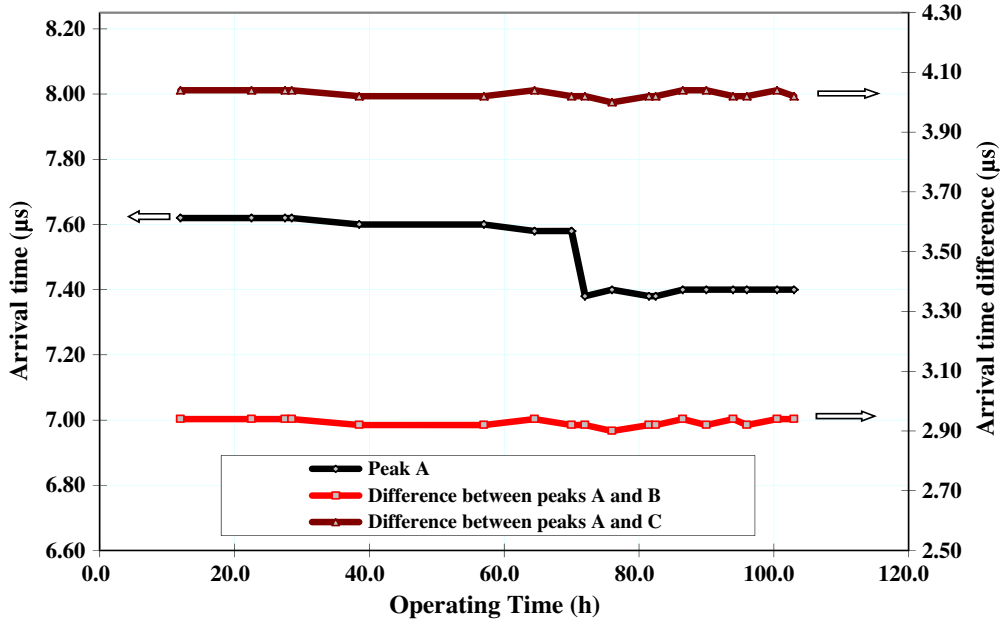

Fig. 4. Arrival time for peak A (left ordinate) and the difference between the arrival times for peaks B and A, and for peaks C and A (right ordinate) as a function of operating time.

point measurement, it can provide a far more sensitive indicator of fouling than integral measures such as flux decline or transmembrane pressure increase.

The last three columns in Table 1 summarize the arrival times for peaks A, B, and C. Note that the difference between the arrival times of peaks B and C is 1.10 ± 0 s for the entire 27.5 h during which the feed was deionized distilled water. Based on a value of 1,500 m/s for the speed of sound in water, this corresponds to a distance of 825 ± 0 μm, which agrees reasonably well with the nominal value of 710 μm given for the feed channel spacer thickness of the 2521 spiral-wound module (Fig. 1). Hence, this correspondence supports the supposition that peaks B and C correspond to the outer and inner membrane layers, respectively, of the outermost feed channel of the 2521 spiral-wound module.

Fig. 4 is a plot of the arrival time of peak A (left ordinate) and the arrival time difference between peaks B and A, and between peaks C and A (right ordinate) vs. the operating time (note that the scales for the left and right ordinates are different). Note that peak A corresponds to the outer wrapping, which is not affected by the calcium sulfate fouling. However, the arrival time for peak A is seen to decrease by 0.02 μs between 28.5 and 38.5 h, and by 0.20 μs between 70 and 72 h. Based on a value of 1,500 m/s for the speed of sound in water, the total decrease in transit time of 0.22 μs indicates that the dead space/wrapping interface has been displaced in a radial direction such that it is 165 μm closer to the outer surface of the module housing. Fig. 4 shows that the difference between the arrival times of peaks A and B remained constant at 2.93 ± 0.01 μs and that between peaks A and C remained constant at 4.03 ± 0.01 μs. These data imply either displacement of the entire filter element relative to the housing or equal expansion of the wrapping and the outer and inner membranes by 165 μm. Although data from additional transducers would be required to distinguish between these alternatives, these results indicate the utility of arrival time analysis for insights regarding module operation unrelated to fouling.

It might seem surprising that the fouling detected by the UTDR amplitude data in Table 1 did not cause any measureable change in the spacer channel thickness throughout the entire fouling and cleaning cycle. Since peaks B and C correspond to the outer and inner membranes for the outermost feed channel in the 2521 spiral-wound module, fouling should cause the transit time for peak B to increase and that for peak C to decrease. Note that a fouling layer having a thickness of 20 μm would cause a change of less than 0.01 μs in the arrival time for peaks B and C. The effect of fouling layer deposition on the transit time is completely masked by the 165 μm displacement of envelope layers. Some prior studies have attempted to infer the thickness of the fouling layer on the membrane by the change in transit time for the waveform reflection from the fouled membrane surface. The results presented here indicate that it is critical to determine if there is any displacement of the membrane envelope layers in the spiral-wound module, since this can cause a much larger decrease in the transit time than the buildup of the fouling layer. It is standard practice when using UTDR to detect membrane fouling to reference the reflected waveform from the fouled membrane to the reflection from some fixed surface. It is important that this reference be a surface that is unaffected by the fouling and not differentially affected by any displacement of the filter layers.

3.2. Fouling and concentration polarization

Fouling is usually inferred from either a decrease in permeate flux and/or salt rejection or an increase in the transmembrane pressure. However, these can change for reasons other than fouling such as concentration polarization and/or membrane compaction. One would like to distinguish between changes caused by concentration polarization and those caused by membrane fouling, since only the latter ultimately requires some type of remedial action. In order to assess whether UTDR detection of membrane fouling would be compromised by concentration polarization, a test was done on a 2521 spiral-wound module whereby an initial deionized distilled water feed was abruptly changed after 1.5 h of operating time to an aqueous solution of 2.1 g/L of sodium chloride. Then at an operating time of 6.5 h, the feed was abruptly switched back to deionized distilled water. Table 2 summarizes the normalized permeation flux, retentate salt concentration, and normalized UTDR amplitude as a function of operating time. Fig. 5 plots the normalized flux and normalized UTDR amplitude of peak C on the left ordinate and the NaCl concentration on the right ordinate (note the different ordinate scales) as a function of the operating time. The initial switch to a salt solution feed (shown by the vertical dotted line on the left in Fig. 5) caused a gradual increase in the retentate salt concentration, whereas switching back to a deionized distilled water feed (shown by the vertical dotted line on the right in Fig. 5) caused a gradual decrease in the retentate salt concentration. A marked decrease in the permeation flux is observed to track the increase in NaCl concentration owing to the concentration polarization.

Table 2
Normalized permeate flux, NaCl concentration in the feed, and normalized UTDR amplitude as a function of operating time during which the feed was abruptly switched at 1.5 h from deionized distilled water to an aqueous NaCl solution and then abruptly switched at 6.5 h back to deionized distilled water at a pressure of 0.68 MPa and temperature of 20˚C

Phase	Time (h)	Normalized flux (%)	NaCl concentration in feed (g/L)	Normalized UTDR amplitude (%)
H_2O	0	100.0	0	100.0
	1.5	101.4	0	102.5
Aqueous NaCl	2.0	92.0	0.304	102.0
	2.5	83.6	0.674	101.9
	3.0	76.1	1.035	102.3
	3.5	69.5	1.362	102.4
	4.5	61.0	1.775	101.8
	6.5	58.7	2.112	106.2
	7.0	58.7	2.112	102.1
	7.5	70.4	1.515	103.8
	8.0	75.6	1.246	103.1
	9.0	83.1	0.894	103.1
	10.0	88.7	0.637	103.8
	12.0	96.2	0.347	101.3
	15.5	101.4	0.156	100.2
	19.5	105.2	0.029	100.2

However, the UTDR amplitude remains constant at 101.8 ± 0.9 g/L throughout the entire 19.5 h of the test. This clearly establishes that the UTDR response is not confounded by concentration polarization. While in principle, the higher salt concentration associated with a concentration polarization boundary layer would result in a correspondingly higher acoustic velocity, the resolution of the relatively low frequency transducer required to penetrate the spiral-wound module is insufficient to detect this effect. As such, UTDR can be used to determine when fouling rather than concentration polarization causes the flux decline.

3.3. Temperature and pressure effects on UTDR response

Preliminary experiments were conducted to demonstrate that temperature and pressure effects could complicate interpretation of the UTDR response. This is a potentially important consideration given that ultrasonic velocity and amplitude can vary with respect to changes in these important operating parameters. Such changes should be relatively small, but have not been extensively characterized for spiral-wound membrane modules. The range of operating conditions considered was 0–2.7 MPa (0–400 psig) for the transmembrane pressure, 10–25˚C for the temperature, and 0.74 g/L for the aqueous $CaSO_4$ feed concentration. Table 3 summarizes the absolute amplitude (mV) of peak C emanating from the inner membrane of the outermost feed channel in the 2521 spiral-wound module as a function of the feed temperature and transmembrane pressure. Fig. 6 shows a plot of the amplitude of peak C in mV vs. the temperature in˚C at a pressure of 0.09 MPa (13 psi) (left ordinate and lower abscissa) and vs. pressure in MPa at a temperature of 20˚C (right ordinate and upper abscissa). As a result of these systematic stepped changes in temperature and pressure, the amplitude of peak C increases monotonically with an increase in temperature and decreases monotonically with an increase in pressure.

In the absence of any effects on the material properties of the layer media, the amplitude should not be significantly affected by the changes in pressure. However, an increase in amplitude with increasing pressure might be expected to the extent that higher pressure causes compression (compaction) of one or more of the layers. The situation with respect to temperature is somewhat more complex since material properties of the polymeric layers do depend upon temperature, and increased absorption at higher temperatures would most likely result in decreased amplitude. However, the temperature range considered here is sufficiently small that any such changes should likewise be relatively small. Thus, the distinct trends indicated in Fig. 6 are more likely due to changes in the morphology of the reflecting surface as a result of fouling.

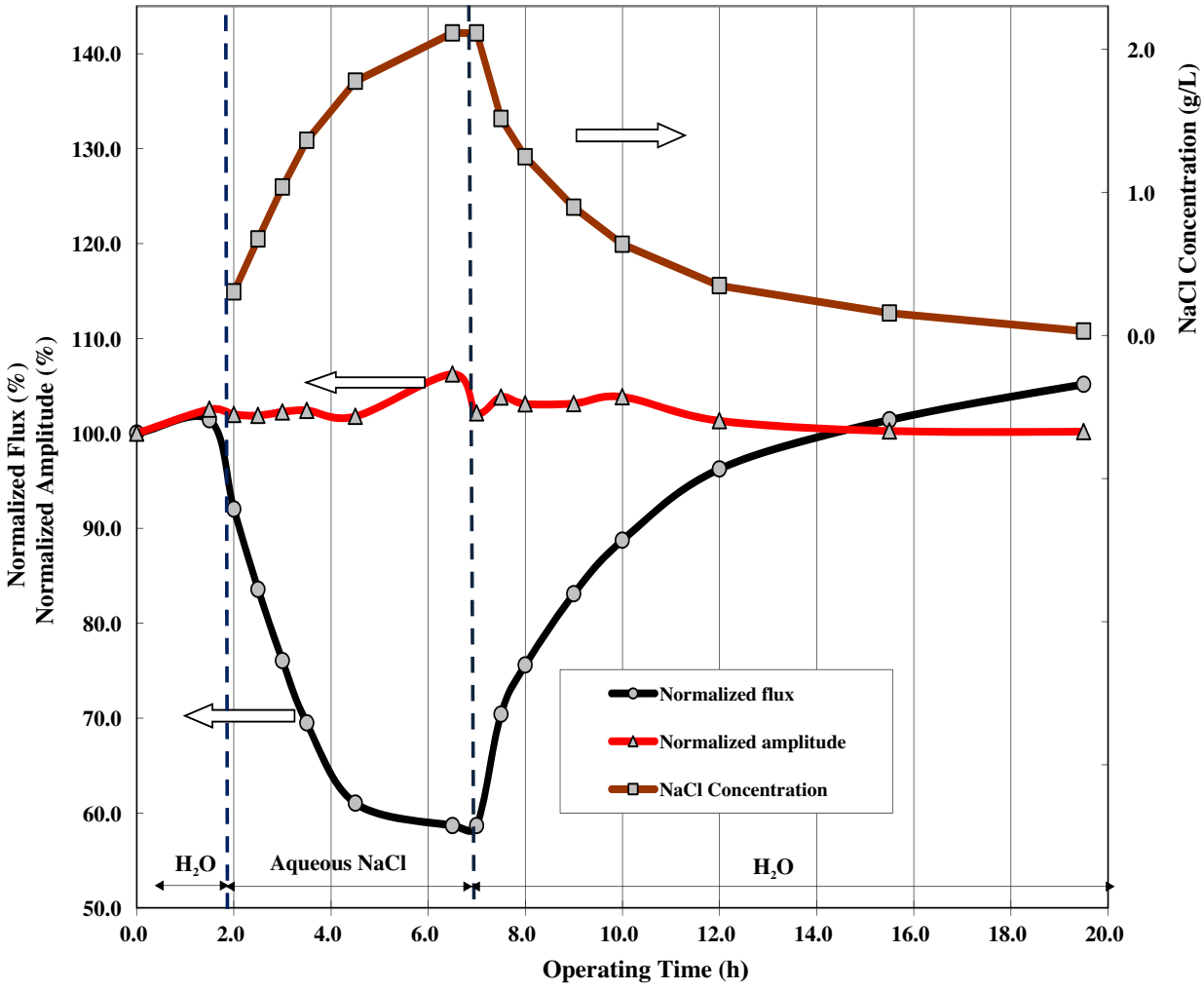

Fig. 5. Normalized permeation flux and normalized UTDR waveform amplitude for peak C (left ordinate) and NaCl concentration (right ordinate) as a function of time at a pressure of 0.68 MPa and temperature of 20°C. The feed was deionized distilled water until 1.5 h (vertical dotted line on left), at which time the it was switched to a solution of 2.1 g/L of NaCl that caused concentration polarization; at 6.5 h, (vertical dotted line on right) the feed was switched back to deionized distilled water that progressively swept out the NaCl. The permeation flux decreases owing to the concentration polarization, whereas the UTDR amplitude remains constant.

Table 3
Effect of transmembrane pressure at a temperature of 20°C and temperature at a pressure of 0.09 MPa (13 psi) on the amplitude (mV) of Peak C corresponding to the inner membrane of the outermost feed channel in the 2521 spiral-wound module

Temperature (°C)	Pressure, MPa (psi)				
	0 (0)	0.09 (13)	0.69 (100)	1.55 (225)	2.75 (400)
10		56.6			
15		70.5	62.7		
20	92.7	86.0	75.2	63.0	36.6
23		91.6			
25			97.6		

Prior studies have shown that dendritic (needle-like) calcium sulfate crystals that form rapidly when the supersaturation created by concentration polarization is relieved cause a decrease in the UTDR amplitude owing to diffuse reflection of the incident waveform [11,12]. In contrast, planar crystalline structures that form more slowly cause an increase in the UTDR amplitude by providing a relatively smooth surface for reflection of the incident waveform [11,12]. The solubility of calcium sulfate dihydrate increases from a value of approximately 1.7 g/L at 0°C to a maximum of slightly more than 2.1 g/L at 40°C, after which it decreases [36]. Hence, the amplitude increase with increasing temperature can be explained by the

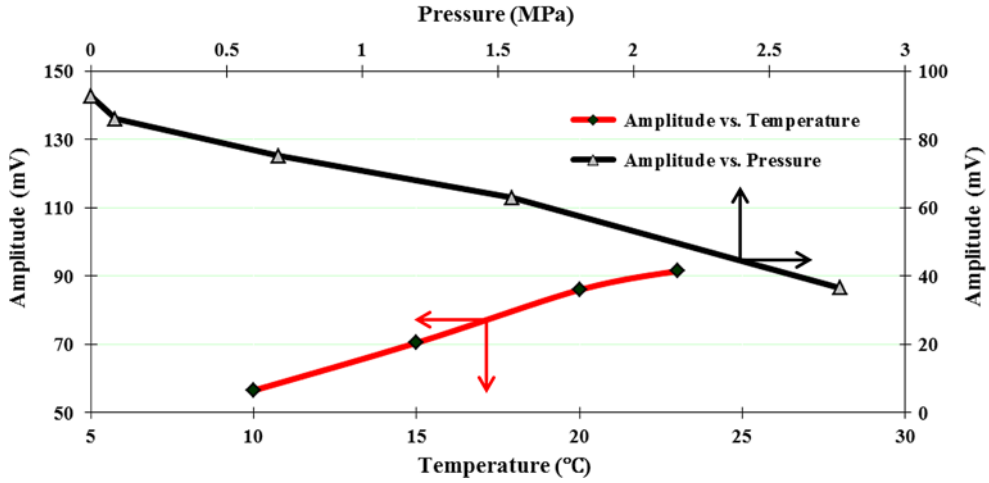

Fig. 6. UTDR waveform amplitude of peak C as a function of temperature at a pressure of 0.09 MPa (13 psi) (left ordinate and lower abscissa) and as a function of pressure at a temperature of 20°C (right ordinate and upper abscissa).

increased solubility that causes a decrease in the crystallization rate that in turn will result in the growth of a larger, more planar crystalline structure that reflects the UTDR waveform more robustly. However, any change in the solubility owing to the pressure increase over the range of 0–2.7 MPa (0–400 psi) would be negligible. The amplitude decrease with increasing pressure is caused by the increase in permeation flux that in turn increases the rate of crystallization and thereby creates a dendritic morphology that results in diffuse reflection of the incident UTDR waveform. These results underscore the importance of maintaining good temperature and pressure control when UTDR is used to infer membrane fouling, and provide a compelling rationale for comprehensive experiments designed to quantify the effects of operating condition changes on UTDR waveforms.

The contention that UTDR amplitude is markedly sensitive to the morphology of the fouling deposits is supported by the fouling interval experiments described in Mairal et al. [12]. This set of experiments was conducted using a Dow BW30 polyamide membrane in a flat sheet module such that the experiments could be interrupted at different times in order to carry out scanning electron microscopy (SEM) analysis of calcium sulfate fouling deposits. The temperature, transmembrane pressure, axial velocity, and $CaSO_4$ feed concentration were held constant at 25°C, 4.14 MPa, 9.8 cm/s, and 0.5 g/L, respectively. Fig. 7 shows SEMs of the fouled membrane surface taken after 90 min (a), 245 min (b), and 290 min (c) and the corresponding plot of the normalized reflected UTDR waveform amplitude as a function of time. The decrease in the UTDR amplitude is seen to correspond to a fouling deposit morphology consisting of patches of dendritic (rosette) crystals (top, left) that progressively spread over the membrane surface (top, center). However, the dendritic crystal structure evolves into a planar morphology that covers much of the entire

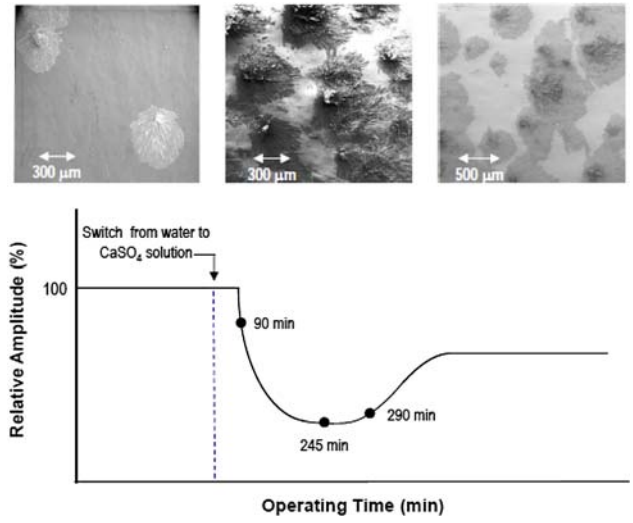

Fig. 7. Corroboration between the reflected UTDR waveform amplitude and fouling layer morphology for $CaSO_4$ fouling on a Dow BW30 polyamide membrane at constant temperature, transmembrane pressure, axial velocity, and feed concentration of 25°C, 4.14 MPa, 9.8 cm/s, and 0.5 g/L, respectively [12]. The upper panels show SEM micrographs of the fouling layer morphology when the experiment was interrupted at 90 (left), 245 (center), and 290 (right) min. The lower panel is a plot of the reflected UTDR waveform amplitude showing the times corresponding to the SEM analyses. The UTDR amplitude decreases as patches of dendritic crystals progressively grow on the membrane surface, and then increases as a planar morphology develops owing to the reduced permeation flux associated with the fouling layer.

surface of the membrane (top, right). This occurs owing to the decrease in the crystallization rate associated with a reduced permeation flux owing to the fouling layer and constant pressure operation.

In summary, a dendritic morphology that arises from rapid crystallization will cause a progressive decrease in the amplitude of the reflected UTDR waveform. In contrast, a planar morphology that is associated with slower crystallization that occurs at smaller permeation fluxes will cause a progressive increase in the amplitude of the reflected UTDR waveform.

4. Conclusions

This study indicates the value of using individual peaks of the reflected UTDR waveform in order to obtain more fundamental information about the fouling process. The amplitude of the reflected UTDR waveform was found to be a more sensitive measure of the fouling than the arrival time at the low fouling rates characteristic of these studies. Interestingly, UTDR revealed that significant displacement of the 2521 spiral-wound module occurred during the operation. When using UTDR to infer membrane fouling, it is critical to use a reference peak based on a surface that is not subject to the fouling and will not move if displacement occurs. If this is not done, the change in transit time could be misinterpreted as being due to the build-up of a fouling layer.

Conventional indicators of fouling such as permeate flux will experience a decline owing to concentration polarization, which cannot be distinguished from that caused by membrane fouling. Hence, flux decline might be incorrectly interpreted to indicate fouling that would require remedial action. In contrast, UTDR is not compromised by concentration polarization and responds only to membrane fouling, and thereby will dictate cleaning only when the membrane is actually fouled.

Results from this study are in agreement with previous work indicating that changes in amplitude of the UTDR waveform in response to membrane fouling depend on the nature of the reflecting interface. Indeed, the observed UTDR amplitude increase in this work underscores the need to quantify and differentiate waveform effects due to operating conditions as distinct from surface changes due to fouling. The effect of increasing temperature on the UTDR response during fouling is likely due to an increase in calcium dihydrate solubility and a corresponding decrease in the rate of crystallization. In contrast, the amplitude of the UTDR response will decrease with increasing pressure owing to an increase in the permeation flux that causes an increase in the rate of crystallization. More rapid crystallization favors the formation of a dendritic morphology that causes diffuse reflection of the UTDR waveform. Slow crystallization favors the formation of larger crystals and a more planar morphology that causes a more robust reflection of the UTDR waveform.

UTDR is finding increasing application for *in situ* characterization of fouling and for fouling detection in conjunction with membrane process control. In view of this, these observations and insights indicate a clear need to quantify the effects of the various factors that affect the real-time waveforms.

Symbols

A	—	acoustic impedance defined by Eq. (1)
c_i	—	speed of sound in medium i
Z_1	—	acoustic impedance of the medium from which the waveform is propagating
Z_2	—	acoustic impedance of the medium into which the waveform is propagating

Greek

ρ_i	—	mass density of medium i

Acknowledgments

During the preparation of this manuscript, Professor Guo-Yong Chia, the first author, passed away. Her coauthors acknowledge her exceptional research accomplishments, in particular her efforts in pioneering the use of ultrasound for studying membranes and membrane processes. We shall miss the wisdom and insight that she brought to our collaborations. This paper is dedicated to her memory.

References

[1] A. Antony, J.H. Low, S. Gray, A.E. Childress, P. Le-Clech, G. Leslie, Scale formation and control in high pressure membrane water treatment systems: A review, J. Membr. Sci. 383 (2011) 1–16.
[2] J. Krautkramer, H. Krautkramer, Ultrasonic Testing of Materials, 4th ed., Springer-Verlag, Berlin, 1990.
[3] A.R. Greenberg, W.B. Krantz, UTDR-based sensors for real-time quantification of membrane module fouling and cleaning, Fluid Part. Separ. J. 15 (2003) 43–49.
[4] W.B. Krantz, A.R. Greenberg, Membrane characterization by ultrasonic time-domain reflectometry, In: N.N. Li, A.G. Fane, W.S.W. Ho, T. Matsuura (Eds.), Advanced Membrane Technology and Applications, John Wiley & Sons, New York, NY, 2008, pp. 879–897.
[5] L.J. Bond, A.R. Greenberg, A.P. Mairal, G. Loest, J.H. Brewster, W.B. Krantz, Real-time nondestructive characterization of membrane compaction and fouling, in: D.O. Thompson, D. E. Chimenti, Review of Progress in Quantitative Nondestructive Evaluation, vol. 14, Plenum, New York, NY, 1995, pp. 1167–1173.
[6] R.A. Peterson, A.R. Greenberg, L.J. Bond, W.B. Krantz, Use of ultrasonic TDR for real-time noninvasive measurement of compressive strain during membrane compaction, Desalination 116 (1998) 115–122.

[7] V.E. Reinsch, A.R. Greenberg, S.S. Kelley, R. Peterson, L.J. Bond, A new technique for the simultaneous, real-time measurement of membrane compaction and performance during exposure to high-pressure gas, J. Membr. Sci. 171 (2000) 217–228.
[8] P. Aerts, A.R. Greenberg, R. Leysen, W.B. Krantz, V.E. Reinsch, P.A. Jacobs, The influence of filler concentration on the compaction and filtration properties of zirfon composite ultrafiltration membranes, Sep. Purif. Technol. 22–23 (2001) 663–669.
[9] S.S. Kelley, A.R. Greenberg, J. Filley, R. Peterson, W.B. Krantz, Chemical modification of cellulose acetate with titanium isopropoxide, Int. J. Polym. Anal. Ch. 7 (2002) 162–180.
[10] W.F.C. Kools, S. Konagurthu, A.R. Greenberg, L.J. Bond, W.B. Krantz, T. van den Boomgaard, H. Strathmann, Use of ultrasonic time-domain reflectometry for real-time measurement of thickness changes during evaporative casting of polymeric films, J. Appl. Polym. Sci. 69 (1998) 2013–2019.
[11] A.P. Mairal, A.R. Greenberg, W.B. Krantz, L.J. Bond, Real-time measurement of inorganic membrane fouling in RO desalination using ultrasonic time-domain reflectometry, J. Membr. Sci. 159 (1999) 185–196.
[12] A.P. Mairal, A.R. Greenberg, W.B. Krantz, Investigation of membrane fouling and cleaning using ultrasonic time-domain reflectometry, Desalination 130 (2000) 45–60.
[13] R.D. Sanderson, J.X. Li, L.J. Koen, L. Lorenzen, Ultrasonic time-domain reflectometry as a non-destructive visualization technique to monitor fouling and cleaning on reverse osmosis membranes, J. Membr. Sci. 207 (2002) 105–117.
[14] J.X. Li, L.J. Koen, D.K. Hallbauer, L. Lorenzen, R.D. Sanderson, Interpretation of calcium sulfate deposition on reverse osmosis membranes using ultrasonic measurements and a simplified model, Desalination 186 (2005) 227–241.
[15] T.H. Chong, F.S. Wong, A.G. Fane, Fouling in reverse osmosis: Detection by non-invasive techniques, Desalination 204 (2007) 148–154.
[16] Zh.-X. Zhang, A.R. Greenberg, W.B. Krantz, G.-Y. Chai, Study of membrane fouling and cleaning in spiral wound modules using ultrasonic time-domain reflectometry, in: A.A. Butterfield, D. Bhattacharyya, New Insights into Membrane Science and Technology: Polymeric, Inorganic and Biofunctional Membranes, Elsevier, Amsterdam, 2003, pp. 65–88.
[17] G.-Y. Chai, A.R. Greenberg, W.B. Krantz, Ultrasound, gravimetric, and SEM studies of inorganic fouling in spiral-wound membrane modules, Desalination 208 (2007) 277–293.
[18] G.H. An, J.G. Lin, J.X. Li, X.Q. Jian, In situ monitoring of membrane fouling in spiral-wound RO modules by UTDR with a sound intensity modeling, Desalin. Water Treat. 32 (2011) 226–233.
[19] G.H. An, J.G. Lin, J.X. Li, X.Q. Jian, Non-invasive measurement of membrane scaling and cleaning in spiral-wound reverse osmosis modules by ultrasonic time-domain reflectometry with sound intensity calculation, Desalination 283 (2011) 3–9.
[20] Z.S. Zhang, V.M. Bright, A.R. Greenberg, Use of capacitive microsensors and ultrasonic time-domain reflectometry for in-situ quantification of concentration polarization and membrane fouling in pressure-driven membrane filtration, Sens. Actuators B. 117 (2006) 323–331.
[21] K.D. Cobry, Z. Yuan, J. Gilron, V.M. Bright, W.B. Krantz, A. R. Greenberg, Comprehensive experimental studies of early-stage membrane scaling during nanofiltration, Desalination 283 (2011) 40–51.
[22] J. Li, J. Liu, T. Yang, C. Xiao, Quantitative study of the effect of electromagnetic field on scale deposition on nanofiltration membranes via UTDR, Water Res. 41 (2007) 4595–4610.
[23] Y.L. Hou, Y.A. Gao, Y. Cai, X.C. Xu, J. Li, In-situ monitoring of inorganic and microbial synergistic fouling during nanofiltration by UTDR, Desalin. Water Treat. 11 (2009) 15–22.
[24] J.X. Li, R.D. Sanderson, G.Y. Chai, D.K. Hallbauer, Development of an ultrasonic technique for *in situ* investigating the properties of deposited protein during crossflow ultrafiltration, J. Colloid Interface Sci. 284 (2005) 228–238.
[25] J.X. Li, R.D. Sanderson, G.Y. Chai, A focused ultrasound sensor for *in situ* detection of protein fouling on tubular ultrafiltration membranes, Sens. Actuators, B. 114 (2006) 182–191.
[26] J.X. Li, R.D. Sanderson, E.P. Jacobs, Non-invasive visualization of the fouling of microfiltration membranes by ultrasonic time-domain reflectometry, J. Membr. Sci. 201 (2002) 17–29.
[27] J.S. Li, R.D. Sanderson, In situ measurement of particle deposition and its removal in microfiltration by ultrasonic time-domain reflectometry, Desalination 146 (2002) 169–175.
[28] X.C. Xu, J.X. Li, H.S. Li, Y. Cai, Y.H. Cao, B.Q. He, Y.Z. Zhang, Non-invasive monitoring of fouling in hollow fiber membrane via UTDR, J. Membr. Sci. 326 (2009) 103–110.
[29] R.D. Sanderson, J.X. Li, D.K. Hallbauer, S.K. Sikder, Fourier wavelets from ultrasonic spectra: A new approach for detecting the onset of fouling during microfiltration of paper mill effluent, Environ. Sci. Technol. 39 (2005) 7299–7305.
[30] S.K. Sikder, M.B. Mbanjwa, D.A. Keuler, D.S. McLachlan, F.J. Reineke, R.D. Sanderson, Visualisation of fouling during microfiltration of natural brown water by using wavelets of ultrasonic spectra, J. Membr. Sci. 271 (2006) 125–139.
[31] S.H.D. Silalahi, T. Leiknes, J. Ali, R.D. Sanderson, Ultrasonic time domain reflectometry for investigation of particle size effect in oil emulsion separation with crossflow microfiltration, Desalination 236 (2009) 143–151.
[32] S.T.V. Sim, T.H. Chong, W.B. Krantz, A.G. Fane, Monitoring of colloidal fouling and its associated metastability using ultrasonic time domain reflectometry, J. Membr. Sci. 401–402 (2012) 241–253.
[33] X.-Y. Lu, E. Kujundzic, G. Mizrahi, J. Wang, K. Cobry, M. Peterson, J. Gilron, A.R. Greenberg, Flow reversal controlled by ultrasonic sensors in RO desalination: Part 1. Mitigation of calcium sulfate scaling, J. Membr. Sci. 20–32 (2012) 419–420.
[34] G. Mizrahi, K. Winata, X-Y Lu, E. Kujundzic, A.R. Greenberg, J. Gilron, Flow reversal controlled by ultrasonic sensors in RO desalination: Part 2. Mitigation of calcium carbonate scaling, J. Membr. Sci. 9–19 (2012) 419–420.
[35] E. Kujundzic, A.R. Greenberg, R. Fong, B. Moore, D. Kujundzic, M. Hernandez, Biofouling potential of industrial fermentation broth components during microfiltration, J. Membr. Sci. 349 (2010) 44–55.
[36] E.P. Partridge, A.H. White, The solubility of calcium sulfate from 0° to 200°C, Am. Chem. Soc. J. 51 (1929) 360–370.